Laser and Particle Beams (2015), *33*, 765–771.

doi:10.1017/S0263034615000841

Collimated proton beams by ultra-short, ultra-intense laser pulse interaction with a foil–ramparts target

HUAN WANG,[1,2,3] LIHUA CAO,[1,3,4,5] AND X.T. HE[1,3,4,6]

[1]Center for Applied Physics and Technology, Peking University, Beijing 100871, China
[2]Institute of Plasma Physics and Fusion, Peking University, Beijing 100871, China
[3]Key Laboratory of High Energy Density Physics Simulation (HEDPS) of the Ministry of Education, Peking University, Beijing 100871, China
[4]Institute of Applied Physics and Computational Mathematics, Beijing 100088, China
[5]IFSA Collaborative Innovation Center, Shanghai Jiao Tong University, Shanghai 200240, China
[6]Institute for Fusion Theory and Simulation, Zhejiang University, Hangzhou 310027, China

(Received 22 April 2015; Accepted 28 July 2015)

Abstract

A foil–ramparts target interaction with an ultra-short, ultra-intense laser pulse (pulse duration between 10^{-12} and 10^{-15} s, intensity above 10^{18} W cm^{-2}) to produce proton beams with controlled divergence and concentrated energy density in target normal sheath acceleration regime is studied. Two-dimension-in-space and three-dimension-in-velocity particle-in-cell simulations show that the foil–ramparts target helps to reshape the sheath electric field and generate a transverse quasi-static electric field of ~6.7 TV m^{-1} along the inner wall of the ramparts. The transverse electric field suppresses the transverse expansion of the proton beam effectively, as it tends to force the produced protons to focus inwards to the central axis, resulting in controlled divergence and concentrated energy density compared with that of a single plain target. The dependence of proton beam divergence on length of the rampart h is investigated in detail. A rough estimation of h ranges depending on dimensionless parameter a_0 of the incident laser is also given.

Keywords: Foil–ramparts target; Proton beams; TNSA; Particle-in-cell (PIC); Controlled divergence

1. INTRODUCTION

The laser-driven ion acceleration from ultra-short, ultra-intense (USUI) laser pulse (pulse duration between 10^{-12} and 10^{-15} s, and intensity above 10^{18} W cm^{-2}) interaction with various solid targets has been studied actively for applications ranging from basic particle physics (Santala *et al.*, 2001), bench-top particle accelerators (Wilks *et al.*, 2001; Yan *et al.*, 2008; Yan *et al.*, 2009), medical therapies (Bulanova *et al.*, 2008; Ledingham *et al.*, 2003), fast ignition of inertial controlled fusion (Tabak *et al.*, 1994; Roth *et al.*, 2001), etc. Up to now, several mechanisms for accelerating ions have been proposed, such as target normal sheath acceleration (TNSA) (Wilks *et al.*, 2001; Robson *et al.*, 2007), laser breakout afterburner (Yin *et al.*, 2006), and radiation pressure acceleration (Esirkepov *et al.*, 2004). Many potential applications require proton and ion beams with high collimation, monoenergetic, larger particle number, and intense energy density, as a result, the enhancement of beam quality becomes of intriguing interest and numerous experimental and theoretical studies have been devoted to achieve this goal (He *et al.*, 2007; Robinson *et al.*, 2007; Chen *et al.*, 2008*a*; Yan *et al.*, 2008; Yu *et al.*, 2009; Qiao *et al.*, 2013; Wang *et al.*, 2014).

When an intense laser pulse irradiates on a thin plain target, a large number of electrons are accelerated and then transport to the backside of target. An electron cloud is formed and a strong electrostatic charge-separation field is also established there. A population of protons near the rear surface are pulled out and accelerated by the sheath electric field (Wilks *et al.*, 2001; Gibbon, 2004), this mechanism is the so-called TNSA. A spatial local and uniform sheath field at the target rear surface is required for TNSA. However, the ponderomotive force by the laser pulse with transversal distributing would push electrons to the lateral edges; the hot electrons with different lateral expanding velocity will inevitably result in the edge effect. To obtain a collimated proton beam with high quality, some tailored structural targets and ions-doped foil targets were proposed previously by improving the configuration of sheath electric field (Nakamura *et al.*, 2007; Ni *et al.*, 2013).

Address correspondence and reprint requests to: Lihua Cao and X.T. He, Institute of Applied Physics and Computational Mathematics, Beijing 100088, China. E-mail: cao_lihua@iapcm.ac.cn and xthe@iapcm.ac.cn

In this paper, we study a practical scheme to generate proton beams with controlled divergence and concentrated energy in TNSA regime by a USUI laser illuminating the foil–ramparts target, and we also employ a same single plain target without the backside ramparts as a comparison. Two-dimension-in-space and three-dimension-in-velocity (2D3V) particle-in-cell (PIC) simulations demonstrate the effectiveness of the foil–ramparts target in suppressing the transverse proton beam divergence by confining the sheath electric field between the ramparts almost locally and uniformly and also by generating a transverse electric field to focus the protons. Accordingly, the dependence of the proton beam characteristics on the target rampart length is also worthy to investigate in detail.

This work is organized as follows. In Section 2, we present the target model and the simulation parameters. For comparison, both of the single plain and foil–ramparts target are considered. In Section 3, our simulation results are presented, from which one can see the robust improvement on the beam divergence and protons energy density using the foil–ramparts target. The dependence of proton beam divergence on length of the rampart is examined thoroughly in Section 4, as well as some estimations about rampart length range on laser intensity a_0. A conclusion is given in Section 5.

2. TARGET CONFIGURATION AND SIMULATION PARAMETERS

The simulations are performed with a 2D3V PIC code KLAP2D (Chen *et al.*, 2008*b*). In the simulations, 1500 cells longitudinally along the z-axis and 2000 cells transversely along the y-axis constitute a 15×20 μm^2 simulation box, with absorbing boundary conditions for particles. A laser pulse linearly polarized along the y-axis with $a_0 = 6$ (intensity $I_0 \approx 4.9 \times 10^{19}$ W cm^{-2}) and wavelength $\lambda_0 = 1$ μm is incident on a solid plain target comprised of electrons and protons. The front side of the plain target is located at $z = 5$ μm, of which thickness is 1 μm and width is 20 μm. To include the prepulse effect, we employ a linear density gradient in 0.5 μm at the laser illumination surface. Figure 1 shows a conceptual diagram of the single plain target and the foil–ramparts target studied in our simulation. In the case of the single plain target [see Figure 1(a)], the initial electrons and protons peak density is 50 n_c, and the foil–ramparts target is designed to have the same configuration and particle settings with the single plain one, and together with these, two horizontal 5 μm thick, 100 n_c dense ramparts with length of h and interval of 4 μm made up of Al^{3+} and electrons attached behind the foil [see Figure 1(b)]. The initial temperature of electrons is set to be 1000 eV. About $(1.4–2.0 \times 10^6)$ superparticles are employed in our simulations. The laser pulse coming from the left boundary has a transverse Gaussian profile with beam waist $r_0 = 2.5$ μm and a trapezoidal temporal profile of duration $\tau = 22\ T$, consisting of a plateau of 20 T and rising and falling periods of 1 T each, where T is the laser period. As has been studied by Yu *et al.* (2009) and Nakamura *et al.* (2007), the optimal width between the ramparts is of the order of the laser spot size and proton beam divergence and energy characteristics have little dependence on pulse duration; so we fix the laser parameters and rampart width all through this paper.

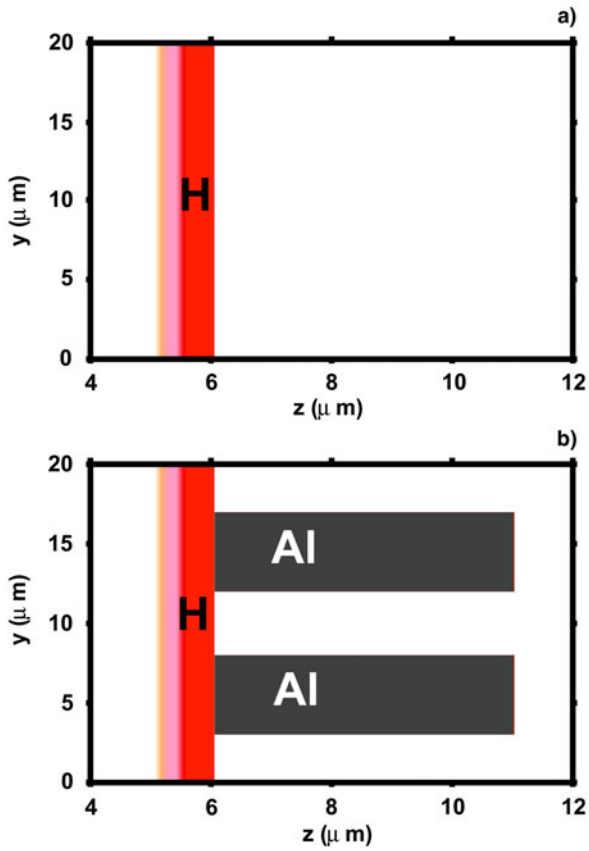

Fig. 1. The conceptual diagram of the single plain target and the foil–ramparts target studied in our simulation. (**a**) The single plain target with the initial electrons and protons peak density of 50 n_c, and (**b**) the foil–ramparts target, which is designed to have the same configuration and particle settings with the single plain one, and together with these, a hole with length of $h = 5$ μm and diameter of 4 μm surrounding by two 5 μm thick, 100 n_c dense horizontal ramparts made up of Al^{3+} and electrons. The front side of the plain target is located at $z = 5$ μm, and its thickness and width are 1 and 20 μm, respectively. To include the prepulse effect, we employ a linear density gradient in 0.5 μm at the laser illumination surface. The initial temperature of electrons is set to be 1000 eV. The target materials have been marked.

3. EFFECT OF FOIL–RAMPARTS TARGET IN RESHAPING SHEATH FIELD AND INDUCING TRANSVERSE ELECTRIC FIELD

The main acceleration mechanism we consider here is TNSA, which means the shape of sheath electric field determined by the accelerated hot electron cloud spread is vital to the quality of the subsequently generated proton beam. Firstly, the shape of sheath electric fields for both plain and foil–ramparts target are investigated. Figures 2(a)–(f) show distributions of cycle-averaged sheath field E_{sheath} (E_{sheath} is actually the longitudinal electric field E_z) at $t = 10$, 20,

https://doi.org/10.1017/S0263034615000841 Published online by Cambridge University Press

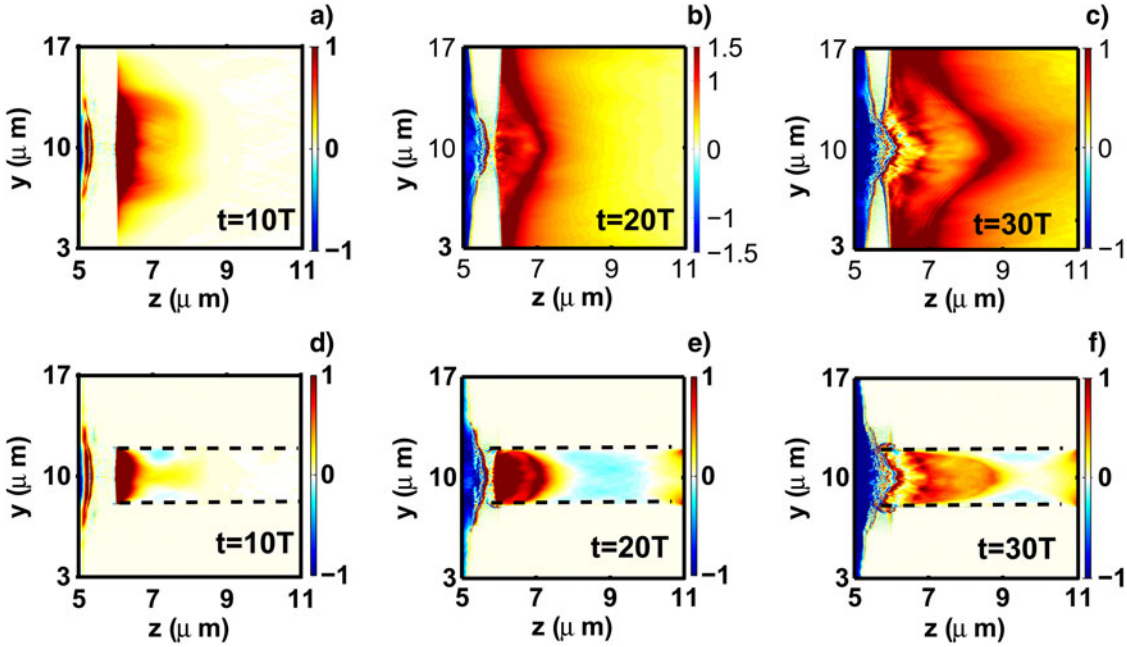

Fig. 2. Distributions of cycle-averaged sheath electric fields E_{sheath} at $t = 10$, 20, and 30 T for plain (**a**)–(**c**) and hole-target (**d**)–(**f**), respectively. The dashed black lines show the initial inner boundaries of the Al ramparts. The electric fields are normalized by $m_e\omega_0 c/e$, where m_e, ω_0, c, and e are the electron rest mass, laser angular frequency, light speed in vacuum, and electron charge, respectively.

and 30 T for plain (top) and foil–ramparts target (bottom), respectively. One can notice that in Figures 2(a)–(c) for the plain target, at early time, say $t = 10$ T, the maximum sheath field $E_{\text{sheath}}^{\text{max}} \sim 1.2 \times 10^{13}$ V m^{-1} is centralized around the laser incident axis with a diameter of about 10.3 λ and the further away from the central axis, the weaker E_{sheath}. As the accelerated hot electrons are further exploding into the vacuum, say at $t = 20$ T, E_{sheath} is expanding along both the transverse and longitudinal directions as well, resulting in a wider and longer bell shape. What's more, E_{sheath} is still y-axial symmetric, but is stronger ($E_{\text{sheath}}^{\text{edges}} \sim 6.6 \times 10^{12}$ V m^{-1}) at the target top and bottom edges than that ($E_{\text{sheath}}^{\text{axis}} \sim 4.5 \times 10^{12}$ V m^{-1}) in the region nearer around laser axis. At later time points $t \geq 30$ T, E_{sheath} has expanded more decentralized, and the maximum sheath field is obviously located at the top and bottom edges of the plain target, leaving the centraxonial E_{sheath} much more weaker. Add it all up, the transverse edge effect of E_{sheath} is one of the reasons which lead to proton beam divergence and large spot size. As shown in Figures 2(d) and (f), in the case of the foil–ramparts target, the transverse edge effect of E_{sheath} is suppressed by the horizontal ramparts made of Al, which forces E_{sheath} to distribute uniformly and locally inside the ramparts, and from our simulation results, we obtain $E_{\text{sheath}} \sim 9.0 \times 10^{12}$, 4.8×10^{12}, 2.1×10^{12} V m^{-1} at $t = 10$, 20, 30 T, respectively. The accelerated hot electrons in the initial proton plain target can transport in the closely behind Al ramparts and propagate forward into the vacuum. These propagating hot electrons can set up the very strong sheath field E_{sheath} at the tip of ramparts and the vacuum, instead of the regions like that of the plain target. This is why the foil–ramparts target can help to eliminate the edge effect.

As the shape of E_{sheath} evolves over time, we pick up three snap shots of sectional view (the cross-section is at $z = 6.5$ μm at the same time points mentioned above), and the results are presented in Figure 3. Compared with E_{sheath} of the plain target (red line), which is much broader and has two sharp corners almost symmetrical about the central axis ($y = 10$ μm), E_{sheath} of the foil–ramparts target (black line) is limited just tightly around central axis, being local and uniform. Moreover, for the single plain target, as we discussed above, the two corners of E_{sheath} are moving outwards to the top and bottom edges of the plain target and meantime the central part of E_{sheath} is getting weaker. The maximum E_{sheath} shown in Figure 3 is smaller for the foil–ramparts target due to less accelerated hot electrons produced between the ramparts than that in vacuum of the plain target rear side.

The foil–ramparts target not only has an advantage over the plain one in controlling the shape of E_{sheath}, but also has a transverse electric field E_y induced between the ramparts which does not exist in the case of the plain target. As one can see in Figure 4, E_y has opposite directions, that is, in the upper side E_y is negatively along $-y$, while in the lower side E_y is positively along $+y$; thus this transverse field tends to focus and confine the protons in the transverse direction as a tight bunch. The transverse electric field can reach as large as 6.43×10^{12} V m^{-1} according to our simulation results, which is approximately consistent with

$$E_y \sim \frac{\Phi_y}{e\lambda_D} \sim \frac{\left(\sqrt{1+a_0^2}-1\right)m_e c^2}{e\lambda_D} = 6.71 \times 10^{12}\ \text{V m}^{-1}.$$

https://doi.org/10.1017/S0263034615000841 Published online by Cambridge University Press

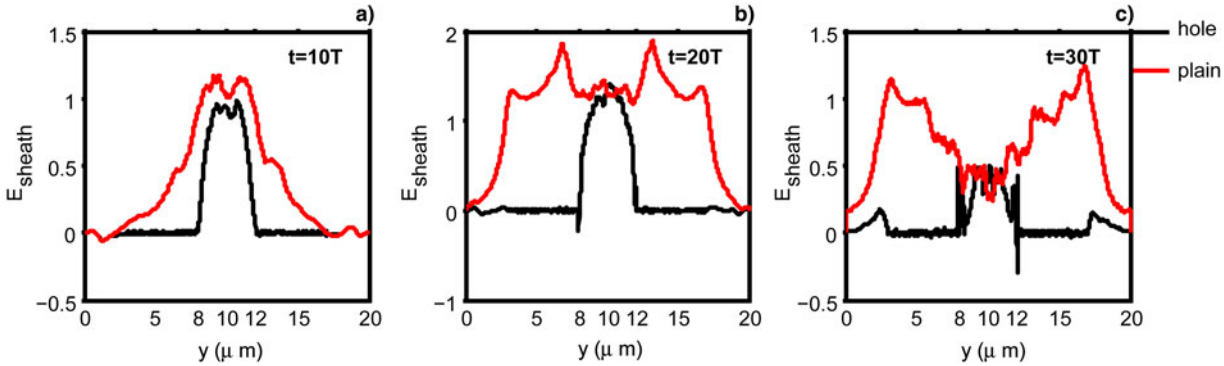

Fig. 3. Sectional view of E_{sheath} for the cross-section located at $z = 6.5$ μm at time points, (**a**) $t = 10\ T$, (**b**) $t = 20\ T$, and (**c**) $t = 30\ T$, where the red line is for the plain target and the black line is for the foil–ramparts target. The electric fields E_{sheath} are cycle-averaged and normalized by $m_e\omega_0 c/e$.

where we estimate $\lambda_D = \sqrt{\epsilon_0 T_e/n_e e^2}$ as the Debye length of accelerated hot electrons with temperature $T_e \approx m_e c^2 \sqrt{1 + 2U_p/m_e c^2} \sim 2.23$ MeV, $a_0 = eE_0/m_e\omega c$ is the dimensionless parameter and ϵ_0 is the vacuum permittivity.

To have a clear understanding about the energy distribution characteristics of generated protons in the rear side of the targets, we use Figure 5 to show the distribution of proton energy density in the region beyond $z = 5$ μm at time $t = 30\ T$ for both plain and foil–ramparts target. One can ensure that thanks to both the reshaped E_{sheath} and the induced transverse electric field E_y, protons produced by the foil–ramparts target have been confined between the ramparts with energy more greatly concentrated compared with that of the plain target.

4. THE DEPENDENCE OF PROTON BEAM DIVERGENCE ON LENGTH OF THE RAMPART

In Section II, when declaring the simulation parameters, we fix the width between the ramparts ($D = 4$ μm) and leave length h as the only geometric variable. Here we investigate the dependence of proton beam divergence on h. Figure 6 demonstrates the rear sheath field E_{sheath} at $t = 30\ T$ at the cross-section $z = 6.5$ μm for the single plain target and foil–ramparts target with different lengths $h = 0.6$, 1, 3, 5, and 7 μm, which are given respectively by lines in different colors as stated in legend. As we have proved above, there is severe edge effect for the plain target, leading to proton divergence. All the foil–ramparts targets have their sheath electric fields limited between the ramparts, except for the difference that the field distributions in the hole formed by the ramparts and on the margin are quite distinct. In the case of $h = 0.6$ μm, marginal sheath field is the strongest among the five foil–ramparts targets, which may result in more accelerated electrons in the marginal region and thus large beam divergence; and furthermore, "marginal effect" makes E_{sheath} fluctuate more wildly between the ramparts. For $h = 1$, 3, 5, and 7 μm cases, the marginal fields are suppressed significantly to equal the level of the electric field between the ramparts, and therefore, the sheath field E_{sheath} is reshaped to be almost uniform and centralized.

Now we focus on the dependence of proton beam divergence on length of the ramparts. Figure 7 shows the

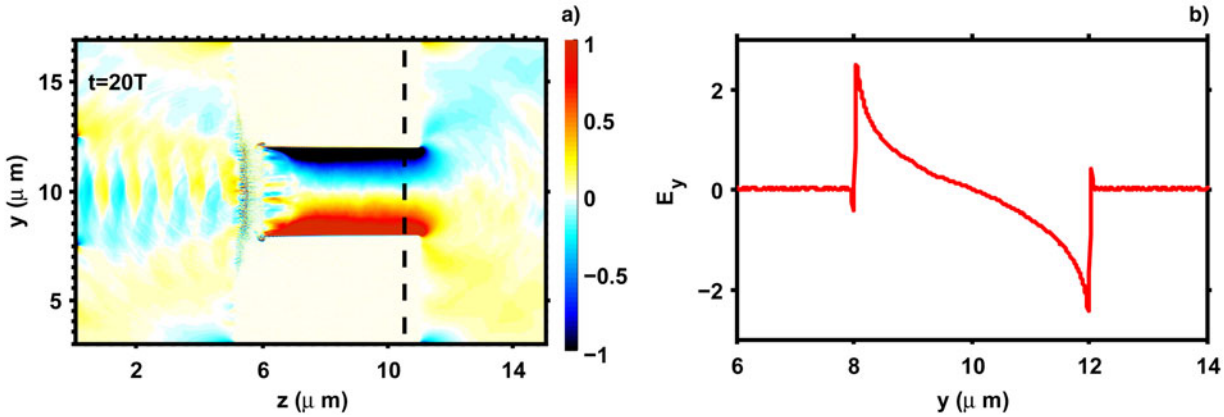

Fig. 4. (**a**) Distribution of transverse electric field E_y in the hole at $t = 20\ T$. (**b**) The sectional view of transverse electric field E_y for the cross-section located at $z = 11$ μm at $t = 20\ T$, where the black dashed line indicates the cross-section. The electric fields E_y are cycle-averaged and normalized by $m_e\omega_0 c/e$.

https://doi.org/10.1017/S0263034615000841 Published online by Cambridge University Press

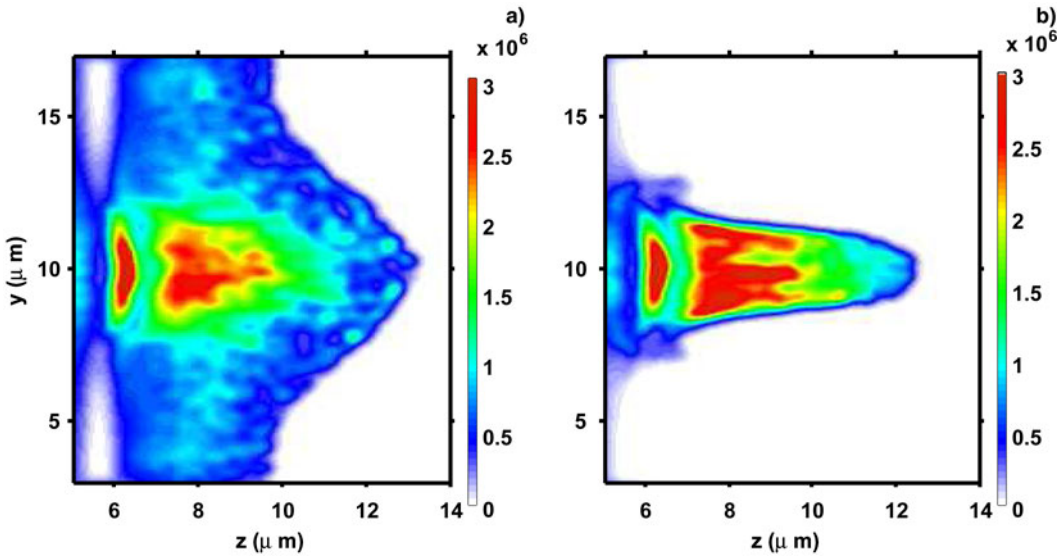

Fig. 5. Distributions of proton energy density in the region $z \geq 5$ μm at $t = 30\ T$ for (**a**) the plain target and (**b**) the foil–ramparts target. Protons' energy density is in unit of $n_e m_e c^2$.

divergence spectrum of accelerated forward-going protons in the rear side ($z > 6$ μm) at $t = 30\ T$ for the single plain target and foil–ramparts target with different lengths $h = 0.6$, 1, and 5 μm. Here divergence angle is defined by the following formula:

$$\theta_{\mathrm{div}} = \arctan \frac{p_y}{p_z},$$

where p_y and p_z are protons transverse and longitudinal relativistic momentum, respectively. One can see clearly that the proton beam from the plain target has two divergence angle peaks in $\theta_{\mathrm{div}} \approx -3.95°$ and 1.91°, while proton beam from the foil–ramparts target with $h = 0.6$ μm has an obvious angular deviation from the central axis and one angle peak in $\theta_{\mathrm{div}} \approx 1.32°$, and proton beams from the foil–ramparts targets with $h = 1$ and 5 μm each has angle peaks in $\theta_{\mathrm{div}} \approx 0.04°$ and 0.19°, respectively. Although the foil–ramparts target with $h = 1$ μm has a smaller peak divergence angle, on the whole its divergence spectrum shape is fatter than foil–ramparts target with $h = 5$ μm. The accelerated proton number in the case $h = 5$ μm from our simulation results is about 9.65×10^9.

So far, we have learned the primary function of the ramparts is to eliminate the electric sheath field "edge effect", confine the accelerated hot electrons and focus the subsequent protons,

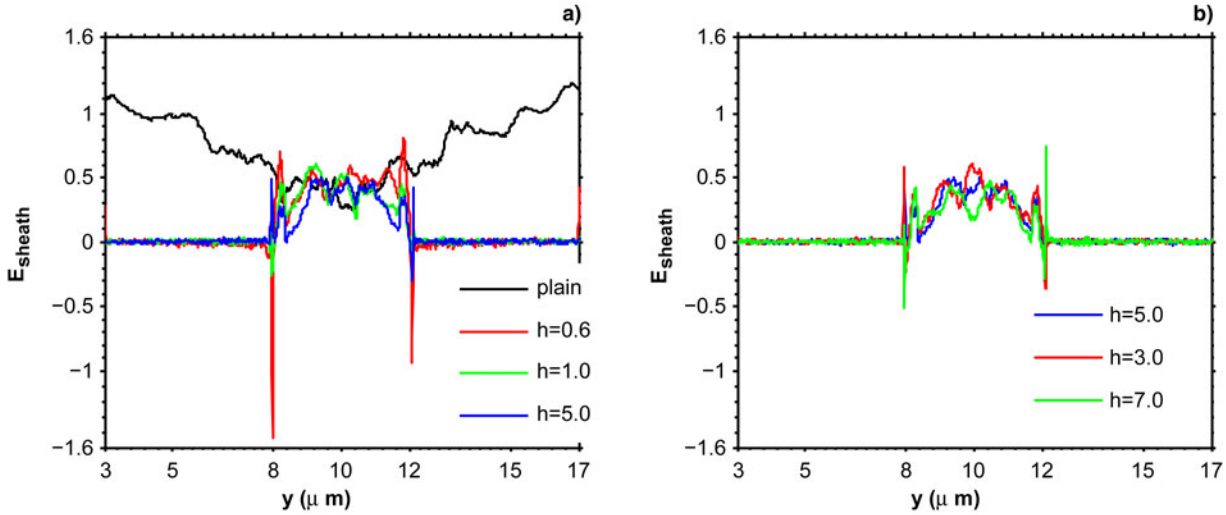

Fig. 6. Distribution of rear sheath electric fields E_{sheath} at $t = 30\ T$ at the cross-section $z = 6.5$ μm: (**a**) for the single plain target and tailored hole-targets with different lengths $h = 0.6$, 1, and 5 μm, where the black line is for the plain target, and the red, green, and blue lines are for $h = 0.6$,1, and 5 μm, respectively; (**b**) for the tailored hole-targets with different lengths $h = 5$, 3, and 7 μm, where the blue, red, and green lines are for $h = 5$, 3, and 7 μm, respectively. The electric fields E_{sheath} are cycle-averaged and normalized by $m_e \omega_0 c/e$.

https://doi.org/10.1017/S0263034615000841 Published online by Cambridge University Press

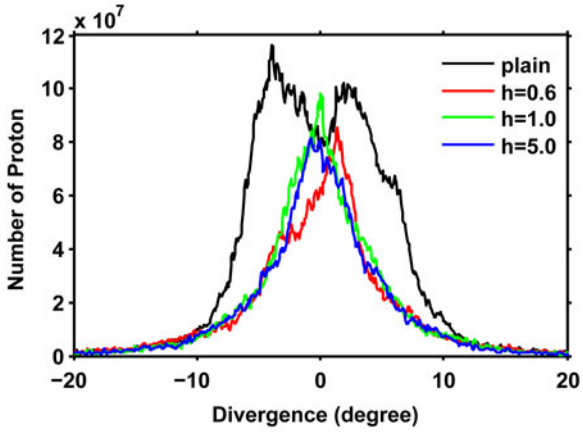

Fig. 7. Divergence spectrum of accelerated forward-going protons in the rear side at $t = 30\ T$ for the single plain target and foil–ramparts target with different lengths, where the black line is for the plain target, and the red, green, and blue lines are for $h = 0.6$, 1, and 5 μm, respectively. The divergence angle is in unit of degree, and the proton number is indicated in the vertical axis.

and we have demonstrated the dependence of proton beam divergence on length of the ramparts, and next, the length range should be figured out. As we know, the accelerated hot electrons temperature is $T_e \approx m_e c^2(1 + 1/2a_0^2)^{1/2}$, and according to the following formula

$$T_e = eE_l L_n,$$

we can estimate the minimum length of the ramparts as the local plasma scale length $h_{min} \sim L_n = C_s t \approx 0.47(1 + 1/2a_0^2)^{1/4}$, where $C_s = \sqrt{T_e/m_i}$ is the ion sound speed, E_l is the longitudinal accelerating field, and t is taken to be the incident laser duration. Now we make some assumptions about the maximum value of h. Wilks *et al.* (2001) found that protons gain energy proportional to the electron temperature,

$$E_p = \alpha T_e = qE_l(\alpha L_n),$$

where q is the proton charge, and α is somewhere between 2 and 12, depending on the model, and from our simulation

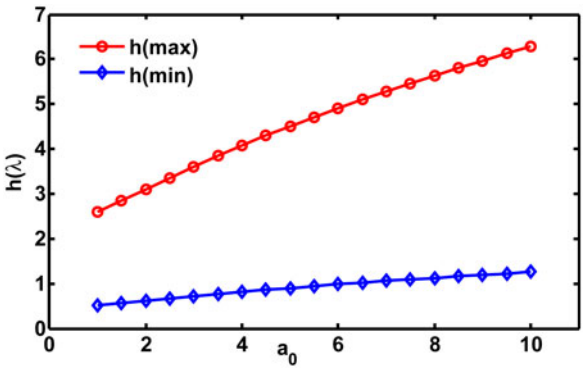

Fig. 8. A rough estimation of the hole length ranges depending on a_0 of the incident laser.

results, we can roughly estimate $\alpha \approx 5$. As a result, by a simple algebraic transformation, we can obtain $h_{max} \sim \alpha C_s t \approx 2.35(1 + 1/2a_0^2)^{1/4}$. Figure 8 shows the estimated range of ramparts length, and we can see using our simulation parameters, $h_{min} \approx 0.98$ μm and $h_{max} \approx 4.91$ μm. It is reasonable that for incident laser with larger a_0, one should use foil–ramparts targets with longer ramparts, and the minimum length shows little change.

5. CONCLUSION

In conclusion, proton acceleration in TNSA regime using a foil–ramparts target has been investigated by 2D3V PIC simulations. It is found that proton beams with intenser energy density and much smaller divergence angle can be produced from suitably picked ramparts length compared with those from the single plain target. The dependence of proton beam divergence on length of the ramparts is also investigated and a rough estimation of the length ranges depending on a_0 of the incident laser is given.

ACKNOWLEDGEMENTS

This work is supported by the Natural Science Foundation of China (Grant numbers 11175030, 11475030, 91230205, 11375032, and 11175029). Huan Wang would like to thank D. Wu for his useful discussions.

REFERENCES

Bulanova, S.V., Esirkepovb, T., Khoroshkovc, V.S., Kuznetsovb, A.V. & Pegorarod, F. (2008). Oncological hadrontherapy with laser ion accelerators. *Phys. Lett. A* **299**, 2–3, 240–247.

Chen, M., Pukhov, A., Sheng, Z.M. & Yan, X.Q. (2008*a*). Laser mode effects on the ion acceleration during circularly polarized laser pulse interaction with foil targets. *Phys. Plasmas* **15**, 113103.

Chen, M., Sheng, Z.M., Zheng, J., Ma, Y.Y. & Zhang, J. (2008*b*). Development and application of multi-dimensional particle-in-cell codes for investigation of laser plasma interactions. *Chin. J. Comput. Phys*. **25**, 43.

Gibbon, P. (2004). *Short Pulse Interactions with Matter*. pp. 180–184. London: Imperial College Press.

He, M.-Q., Dong, Q.-L., Sheng, Z.-M., Weng, S.-M., Chen, M., Wu, H.-C. & Zhang, J. (2007). Acceleration dynamics of ions in shocks and solitary waves driven by intense laser pulses. *Phys. Rev. E* **76**, 035402.

Ledingham, K.W.D., McKenna, P. & Singhal, R.P. (2003). Applications for nuclear phenomena generated by ultra-intense lasers. *Science* **300**, 1107.

Nakamura, M., Kawata, S., Sonobe, R., Kong, Q., Miyazaki, S., Onuma, N. & Kikuchi, T. (2007). Robustness of a tailored hole target in laser-produced collimated proton beam generation. *J. Appl. Phys*. **101**, 113305.

Ni, P.A., Lund, S.M., McGuffey, C., Alexander, N., Aurand, B., Barnard, J.J., Beg, F. N., Bellei, C., Bieniosek, F.M., Brabetz, C., Cohen, R.H., Kim, J., Neumayer, P., Roth, M. & Logan, B.G. (2013). Initial experimental evidence of self-collimation

https://doi.org/10.1017/S0263034615000841 Published online by Cambridge University Press

of target-normal-sheath-accelerated proton beam in a stack of conducting foils. *Phys. Plasmas* **20**, 083111.

Qiao, B., Foord, M.E., Wei, M.S., Stephens, R.B., Key, M., McLean, H. & Beg, F.N. (2013). Dynamics of high-energy proton beam acceleration and focusing from hemisphere-cone targets by high-intensity lasers. *Phys. Rev. E* **87**, 013108.

Esirkepov, T., Borghesi, M., Bulanov, S.V., Mourou, G., & Tajima, T. (2004). Highly efficient relativistic-ion generation in the laser-piston regime. *Phys. Rev. Lett*. **92**, 175003.

Roth, M., Cowan, T.E., Key, M.H., Hatchett, S.P., Brown, C., Fountain, W., Johnson, J., Pennington, D.M., Snavely, R.A., Wilks, S.C., Yasuike, K., Ruhl, H., Pegoraro, F., Bulanov, S.V., Campbell, E.M., Perry, M.D. & Powell, H. (2001). Fast ignition by intense laser-accelerated proton beams. *Phys. Rev. Lett*. **86**, 436.

Robinson, A.P.L. & Gibbon, P. (2007). Production of proton beams with narrow-band energy spectra from laser-irradiated ultrathin foils. *Phys. Rev. E* **75**, 015401.

Robson, L., Simpson, P.T., Clarke, R.J., Ledingham, K.W.D., Lindau, F., Lundh, O., McCanny, T., Mora, P., Neely, D., Wahlstrom, C.-G., Zepf, M. & McKennna, P. (2007). Scaling of proton acceleration driven by petawatt–laser–plasma interactions. *Nat. Phys*. **3**, 58.

Santala, M.I.K., Zepf, M., Beg, F.N., Clark, E.L., Dangor, A.E., Krushelnick, K., Tatarakis, M., Watts, I., Ledingham, K.W.D., McCanny, T., Spencer, I., Machacek, A.C., Allott, R., Clarke, R.J. & Norreys, P.A. (2001). Production of radioactive nuclides by energetic protons generated from intense laser–plasma interactions. *Appl. Phys. Lett* **78**, 19.

Tabak, M., Hammer, J., Glinsky, M.E., Kruer, W.L., Wilks, S.C., Woodworth, J., Campbell, E.M., Perry, M.D. & Mason, R.J. (1994). Ignition and high gain with ultrapowerful lasers. *Phys. Plasmas* **1**, 1626.

Wang, H.Y., Yan, X.Q. & Zepf, M. (2014). Collimated proton acceleration in light sail regime with a tailored pinhole target. *Phys. Plasmas* **21**, 063113.

Wilks, S.C., Langdon, A.B., Cowan, T.E., Roth, M., Singh, M., Hatchett, S., Key, M.H., Pennington, D., MacKinnon, A. & Snavely, R.A. (2001). Energetic proton generation in ultra-intense laser–solid interactions. *Phys. Plasmas* **8**, 542.

Yan, X.Q., Lin, C., Sheng, Z.M., Guo, Z.Y., Liu, B.C., Lu, Y.R., Fang, J.X. & Chen, J.E. (2008). Generating high-current monoenergetic proton beams by a circularly polarized laser pulse in the phase-stable acceleration regime. *Phys. Rev. Lett*. **100**, 135003.

Yan, X.Q., Wu, H.C., Sheng, Z.M., Chen, J.E. & Meyer-ter-Vehn, J. (2009). Self-organizing GeV, nanocoulomb, collimated proton beam from laser foil interaction at 7×10^{21} W/cm^2. *Phys. Rev. Lett.* **103**, 135001.

Yin, L., Albright, B.J., Hegelich, B.M., & Fernandez, J.C. (2006). GeV laser ion acceleration from ultrathin targets: The laser break-out afterburner. *Laser Part. Beams* **24**, 291–298.

Yu, T.P., Ma, Y.Y., Chen, M., Shao, F.Q., Yu, M.Y., Gu, Y.Q. & Yin, Y. (2009). Quasimonoenergetic proton beam from ultraintense-laser irradiation of a target with holed backside. *Phys. Plasmas* **16**, 033112.

https://doi.org/10.1017/S0263034615000841 Published online by Cambridge University Press